Optimization of Oxidative Leaching for Vanadium Extraction from Low-Grade Stone Coal Using Response Surface Methodology

Authors:

Zulv Huang, Tao Chen, Yang Zhou, Wenbin Xu, Hanzhi Lin, Bo Yan

Abstract:

The feasibility and kinetics of vanadium (V) recovery from oxidative leaching of low-grade stone coal using MnO2 were investigated. Oxidative leaching processes (OLPs) were designed using response surface methodology (RSM) based on the central composite design (CCD) model. The results show that the order of factors that influence OLPs is leaching temperature > H2SO4 concentration > leaching time > MnO2 dosage. The interaction between leaching temperature and H2SO4 concentration on the OLP is the most significant. Vanadium leaching efficiency was 89.3% using 31% H2SO4 and 3% MnO2 at 90 °C for 7.9 h. The kinetics of V leaching from stone coal show that the leaching rate is controlled by chemical reaction through a layer according to the shrinking core model and the activation energy is 55.62 kJ/mol. A comparison of the SEM-EDS results of minerals before and after leaching confirms that the muscovite structure was significantly destroyed and V and aluminum (Al) were effectively dissolved during the OLP.

Article

Optimization of Oxidative Leaching for Vanadium Extraction from Low-Grade Stone Coal Using Response Surface Methodology

Zulv Huang [1,2], Tao Chen [3,4,*], Yang Zhou [1,2], Wenbin Xu [5], Hanzhi Lin [1,2] and Bo Yan [3,4]

1. State Key Laboratory of Organic Geochemistry, Guangzhou Institute of Geochemistry, Chinese Academy of Sciences, Guangzhou 510640, China; huangzulv18@mails.ucas.ac.cn (Z.H.); zhouyang173@mails.ucas.ac.cn (Y.Z.); xtulhz@126.com (H.L.)
2. School of Earth and Planetary, University of Chinese Academy of Sciences, Beijing 100049, China
3. SCNU Environmental Research Institute, Guangdong Provincial Key Laboratory of Chemical Pollution and Environmental Safety & MOE Key Laboratory of Theoretical Chemistry of Environment, South China Normal University, Guangzhou 510006, China; bo.yan@m.scnu.edu.cn
4. School of Environment, South China Normal University, University Town, Guangzhou 510006, China
5. Dongjiang Environmental Company Limited, Shenzhen 518000, China; xuwb@dongjiang.com.cn
* Correspondence: tao.chen@m.scnu.edu.cn

check for updates

Abstract: The feasibility and kinetics of vanadium (V) recovery from oxidative leaching of low-grade stone coal using MnO_2 were investigated. Oxidative leaching processes (OLPs) were designed using response surface methodology (RSM) based on the central composite design (CCD) model. The results show that the order of factors that influence OLPs is leaching temperature > H_2SO_4 concentration > leaching time > MnO_2 dosage. The interaction between leaching temperature and H_2SO_4 concentration on the OLP is the most significant. Vanadium leaching efficiency was 89.3% using 31% H_2SO_4 and 3% MnO_2 at 90 °C for 7.9 h. The kinetics of V leaching from stone coal show that the leaching rate is controlled by chemical reaction through a layer according to the shrinking core model and the activation energy is 55.62 kJ/mol. A comparison of the SEM-EDS results of minerals before and after leaching confirms that the muscovite structure was significantly destroyed and V and aluminum (Al) were effectively dissolved during the OLP.

Keywords: vanadium; stone coal; oxidation leaching; optimization; kinetics

1. Introduction

Vanadium (V) is commonly used in the production of alloy steels, catalytic agents, and vanadium batteries. The recovery of vanadium by leaching from stone coal, vanadium titano-magnetite, and waste catalyst has been widely studied [1]. Stone coal is a unique and abundant V resource in China with an estimated reserve of approximately 61.88 billion tons. The total amount of V reaches 118 million tons, which accounts for over 87% of the domestic V reserve [2–5]. With the increasing demand for V-bearing products, V extraction from stone coal has become an important direction for V resource development. However, the average V grade in stone coal is generally low, with only 2.8% of stone coal with grade >1.0% and more than 60% with grade <0.5%. The mining of low-grade stone coal is not economically feasible based on current technology, which leaves a large quantity of low-grade stone coal unexploited (i.e., "dead ore") in China [6,7]. Exploring the feasibility of processes to recover V from low-grade stone coal is, therefore, of great significance to comprehensively develop the use of low-grade stone coal resources in China.

High salt roasting–water leaching is a traditional process to extract V form stone coal, followed by the development of calcification roasting leaching, blank roasting leaching, low-temperature sulfating roasting leaching, as well as a variety of V extraction processes, such as direct acid-leaching technology [6]. Pyrometallurgical methods are gradually losing competitiveness in the treatment of low-grade stone coal owing to high-energy consumption, environmental pollutants, and additional burdens associated with environmental treatment. Direct acid-leaching technology has become a research hotspot for extracting V from low-grade stone coal because of its simple process, environmental protection, solid experimental research foundation, and industrial application prospects [8,9]. Most V in a low oxidation state in stone coal exists in the crystal lattice of aluminosilicate minerals and isomorphically replaces Al(III) in muscovite. The transformation and oxidation of V are, therefore, essential for leaching efficiency [10]. Leaching efficiency can be improved by adding oxygen pressure or oxidants [8,11,12]. However, oxygen pressure leaching is not cost-effective for low-grade stone coal and is only applied to stone coal with a grade higher than 1% to generate an industrially recoverable value [6]. The characteristics of stone coal resources in China and terms of environmental protection and operation make V extraction feasible when assisted by oxidant leaching. Common leaching oxidants are $NaClO_3$, $Na_2S_2O_8$, MnO_2, and O_3 [8,13–15]. However, harmful gases are easily produced during the leaching process of $NaClO_3$ and $Na_2S_2O_8$, and the O_3-assisted leaching process is unstable. In this study, MnO_2 is used as an oxidizer in the leaching process, which is clean, pollution-free, and allows effective recovery of manganese after oxidative leaching processes (OLPs) with excellent industrial application value.

In this study, we established a data model of V extraction from stone coal by an OLP using response surface methodology (RSM) based on the central composite design (CCD) model. The recovery of V by the OLP of stone coal was comprehensively optimized and analyzed. Based on an in-depth discussion of the experimental conditions, the OLP mechanism of V was further studied, including transformation of the mineral lattice and analysis of V leaching kinetics. The kinetics determine the reaction rate and directly affect the engineering and industrial planning of this process [16]. Shrinking core models for spherical particles of a constant size based on the Arrhenius equation are empirically used to study the kinetics of leaching low-grade stone coal. The obtained data are used to calculate leaching activation energies based on kinetic models of the chemical reaction stage. The kinetic model provides theoretical guidance for the application of oxidants in V extraction from low-grade stone coal.

2. Experimental Procedures

2.1. Materials

Stone coal was obtained from Hunan Province in China. The samples were evenly mixed and then crushed to −0.180 mm. The chemical composition of the raw ore is shown in Table 1. The surface morphology of the minerals is shown in Figure 1 from analysis using a scanning electron microscope (SEM, Hitachi SU8010), and the element distribution in minerals was analyzed by an energy-dispersive X-ray spectrometer (EDAX, OCTANESUPER). The energy spectrum analysis of muscovite shows an Al content of 12.02 wt.% in the raw stone coal, which is close to the theoretical Al content of V-bearing muscovite (12.8 wt.%) [17]. The correlation of V, O, Al, Si, and K in raw stone coal indicates that V may exist in the muscovite.

Table 1. Main chemical composition of the stone coal (wt.%).

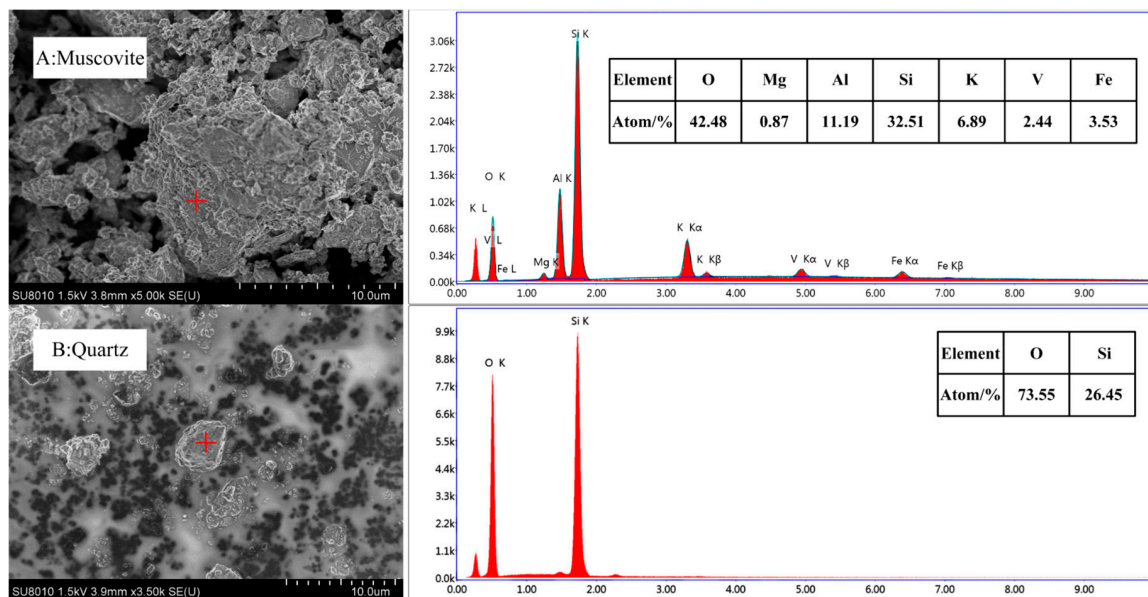| V	Si	Al	K	Na	Mg	Ca	Ba	Fe	Cr	S	Loss
0.30	36.12	2.37	0.56	0.09	0.94	0.05	0.11	0.56	0.05	0.54	11.00

Figure 1. SEM-EDS results of the minerals before leaching: (**A**) muscovite; (**B**) quartz.

2.2. Experimental and Analytical Methods

In the single-factor and optimal experiments, 10-g samples were heated in a water bath with 50 mL of different concentrations of H_2SO_4. The V content of the leaching solution was measured by Chinese standard YB/T 5328-2006, and the V leaching efficiency was calculated by Equation (1). In the kinetic experiments, 50 g of sample and 2 g of MnO_2 were heated and leached with 250 mL of 30% H_2SO_4. The reaction system was stirred at 400 r/min. Solid samples were collected by vacuum filtration at fixed time intervals. After washing and drying, the V content was measured by Chinese standard GB/T 19226-2003. The solid–liquid ratio was held constant during the leaching process, and the V leaching efficiency was calculated by Equation (2).

$$\eta = \frac{C_{vl} \cdot V_l}{C_{vs} M_s} \tag{1}$$

where C_{vl} is the V content of the leaching solution; V_l is the volume of the leaching solution; C_{vs} is the V content of the raw ore sample; and M_s is the mass of the raw ore sample.

$$\eta = 1 \frac{C_a}{C_b} \tag{2}$$

where C_a is the V content of the unit mass residue sample and C_b is the V content of the unit mass raw ore sample.

The experimental results were also entered into Design Expert 10.0 software to fit the model by multiple linear regressions. The CCD regression model can be described as follows:

$$Y = b_0 + \sum_{i=1}^{k} b_i X_i + \sum_{i=1}^{k} b_{ii} X_i^2 + \sum_{i,j=1,\ i \neq j}^{k} b_{ij} X_i X_j \tag{3}$$

where Y is the predicted response (leaching efficiency); b_0 is the constant coefficient; b_i, b_{ii}, and b_{ij} are the linear, quadratic, and interaction coefficients, respectively; X_i and X_j are the coded values of the independent variables; $X_i X_j$ and X_i^2 represent the interaction and quadratic terms, respectively; and k is the number of independent variables (in this study, $k = 4$).

2.3. Optimization of Experimental Design

Both CCD and Box–Behnken design (BBD) can be used in RSM to build a second-order (quadratic) model for the response variables [18]. CCD is more effective than BBD in reflecting the interaction of different variables while the numbers of variables and levels are high (variable number > 3, level number > 3). The total number of required experimental runs was $2^k + 2k + N_0$, where N_0 is the number of replications at the center points ($N_0 = 6$) [19]. We therefore performed thirty experiments corresponding to the four CCD variables. The center points were duplicated to determine the experimental error. The coded levels and range of independent variables for the experimental design are listed in Table 2.

Table 2. Coded levels and range of independent variables for experimental design.

Parameter	Range and Levels				
	−2	−1	0	1	2
A: H$_2$SO$_4$ concentration (%)	8	16	24	32	40
B: leaching temperature (°C)	60	70	80	90	100
C: leaching time (h)	2	4	6	8	10
D: MnO$_2$ dosage (%)	0	1	2	3	4

3. Results and Discussion

3.1. Optimization and Analysis of the Leaching Process

3.1.1. Single-Factor Experiments

Six factors, including leaching temperature, H$_2$SO$_4$ concentration, leaching time, MnO$_2$ dosage, liquid–solid ratio, and stirring rate, were investigated by single-factor experimental sensitivity analysis. The experimental results are shown in Figure 2. V leaching efficiency increases continuously with increasing leaching temperature, H$_2$SO$_4$ concentration, and leaching time. The growth rate of V leaching efficiency slows after 9 h of leaching. V leaching efficiency increases with increasing MnO$_2$ dosage in the range of 1–4%. When the dosage of MnO$_2$ reaches 4%, the V leaching efficiency reaches a maximum of 83.4%. Excessive MnO$_2$ reacts with sulfuric acid and reduces its concentration, resulting in a decrease in V leaching efficiency. The effect of stirring rate on V leaching is not significant. The V leaching efficiency increases by 12.2% when the liquid–solid ratio is increased from 0.5 to 5. An increase in liquid–solid ratio leads to increasing sulfuric acid consumption. Considering the cost and subsequent enrichment process, the liquid–solid ratio was set to 5:1. According to the results of the single-factor experiments, the key variables affecting V leaching efficiency and range of optimal values were determined to be leaching temperature, H$_2$SO$_4$ concentration, leaching time, and MnO$_2$ dosage.

3.1.2. Data Analysis

The analysis of variance (ANOVA) results are presented in Table S1. The Fischer variation ratio (F-value) is a statistically valid measure of how well factors describe data variation about its mean [20]. An F-value of 198.91 implies the model is significant, and there is only a 0.01% chance that an F-value this large could occur due to noise. The R^2 and R^2_{adj} values are 0.9611 and 0.9820, respectively, which are sufficiently high and comparable and indicate that the given quadratic response surface model well describes the experimental data [19]. To obtain an accurate second-order polynomial function, the linear, second-order and interaction of the input variables were evaluated. Values of ($P > F$) that are less than 0.05 indicate significant model terms. In this experiment, the P values of A, B, C, D, AB, BC, A^2, and C^2 are <0.0001, <0.0001, <0.0001, 0.0004, <0.0001, 0.0027, 0.0147, and 0.0039, respectively, which shows that all factors have a significant first-order effect. The effect of each individual factor is as follows: leaching temperature > H$_2$SO$_4$ concentration > leaching time > MnO$_2$ dosage. $AB < 0.0001$ indicates that the intersection of H$_2$SO$_4$ concentration and leaching temperature is extremely apparent

in the OLP. The "Adequate Precision" feature measures the signal to noise ratio. A ratio greater than 4 is desirable in these experiments, and a ratio of 52.120 indicates an adequate signal and that the model can be used to navigate the design space.
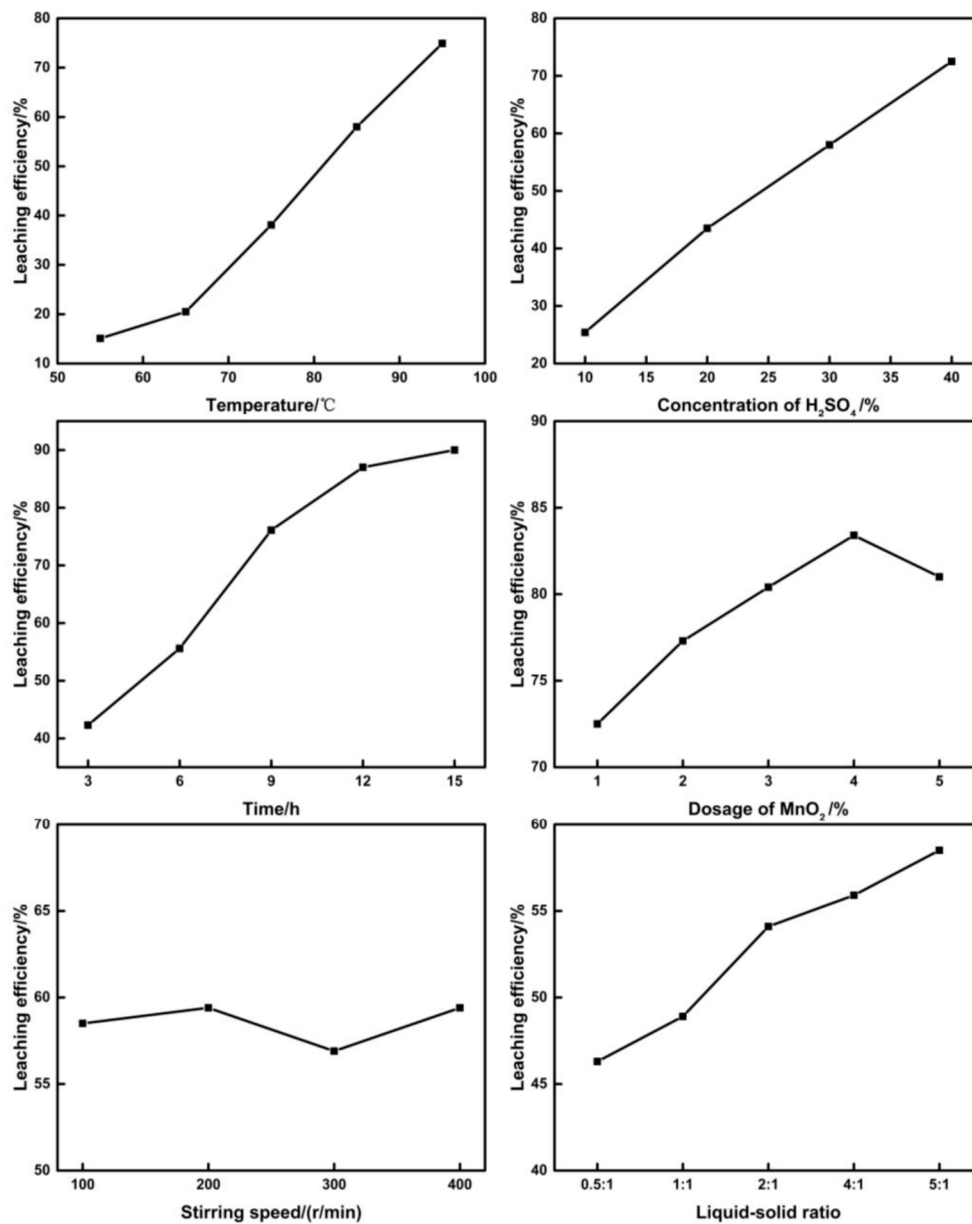

Figure 2. Results of sensitivity analysis of single-factor experiments.

To further evaluate the adequacy of the given quadratic model in fitting the experimental OLP data, an important diagnostic plot of actual versus predicted values was established, as shown in Figure 3. The points are distributed in a straight line that passes through the origin with a slope of 1, which indicates that the quadratic model accurately predicts the actual values. The actual leaching efficiencies of V and Fe are shown in Table S2, according to the experimental design conditions. MnO_2 has a positive effect on V leaching but no discernible effect on Fe leaching. The following regression (Equation (4)) was developed from the CCD results and shows the empirical relationship between V leaching efficiency and the four experimental variables in terms of their coded forms.

$$Y = 49.85 + 11.20A + 15.96B + 9.68C + 2.37D + 4.28AB + 2.33BC - 1.37A^2 - 1.67C^2 \tag{4}$$

where Y is the V leaching efficiency and A, B, C, and D are the coded values of the experimental variables H_2SO_4 concentration, leaching temperature, leaching time, and MnO_2 dosage, respectively.
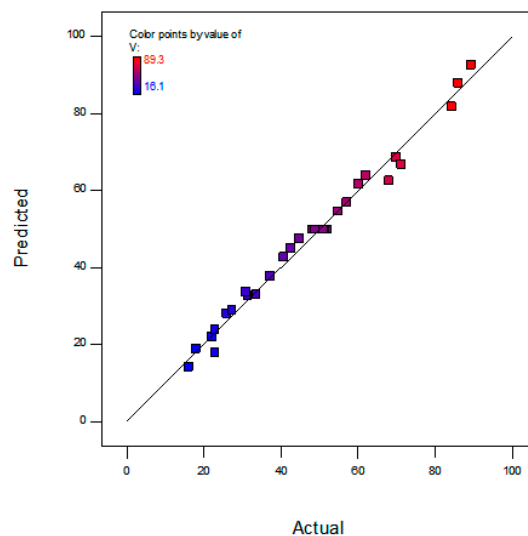

Figure 3. Diagnostic plots of quadratic model (actual versus predicted values).

3.1.3. Internal Relationships between Factors

Interaction terms with *p*-values < 0.05 in the fitted model (*AB* (H_2SO_4 concentration*leaching temperature) and *BC* (leaching temperature*time)) were selected as axes of the response surface plots to account for surface curvature. The interaction implies that the effect produced by changing one variable depends on the level of other variables [19].

The dependence of V leaching efficiency on H_2SO_4 concentration and leaching temperature is shown in Figure 4a, where time and MnO_2 dosage were held constant at 6 h and 2%, respectively. Between 70 and 90 °C, the concentration of H_2SO_4 increased from 16% to 32% and the V leaching efficiency increased by 13.48% and 30.96%, respectively. The effect of increasing H_2SO_4 concentration on leaching is more significant at a high temperature. The ion diffusion rate of the solution increases with increasing leaching temperature, and hydrogen ions entering the mica lattice react more easily. The effect of hydrogen ions destroying mica is enhanced by increasing H_2SO_4 concentration at a high temperature, and the V leaching efficiency significantly increases [21].
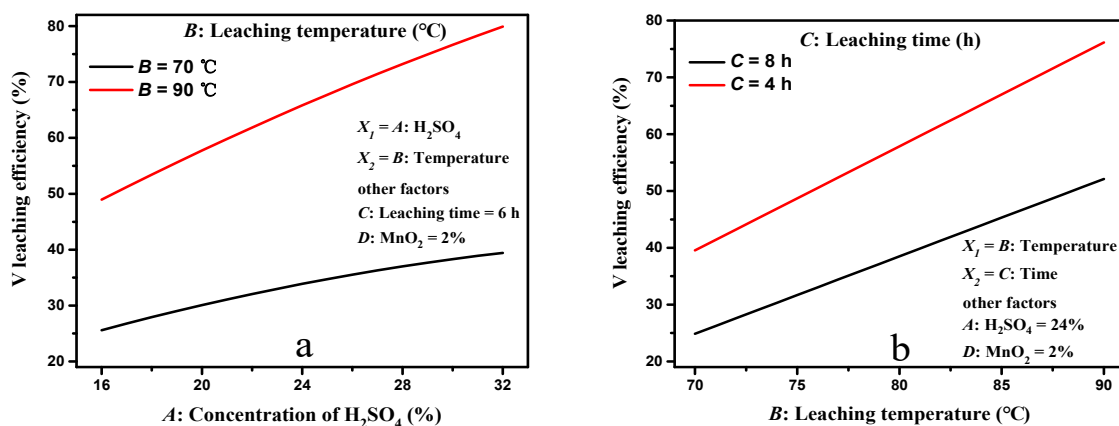

Figure 4. Effect of H_2SO_4 concentration and leaching temperature (**a**) and leaching temperature and time (**b**) on V leaching efficiency.

The dependence of V leaching efficiency on leaching temperature and leaching time is shown in Figure 4b, where H_2SO_4 concentration and MnO_2 dosage are held constant at 24% and 2%, respectively.

A linear relationship is observed between V leaching efficiency and temperature when the leaching time is 4 and 8 h. Longer times are associated with more significant temperature effects on leaching. With increasing leaching temperature, the number of activated molecules increases, the number of effective collisions between molecules increases owing to mutual electron repulsion, and the solution viscosity decreases. Reduced viscosity accelerates the diffusion rate of molecules and ions, which makes it more convenient for hydrogen ions to enter the V-bearing mica lattice and improve the V leaching efficiency [15].

Three-dimensional surface plots and contour plots of the regression model are useful to graphically interpret the associated interactions. Each response surface curve represents the level change of two factors while the remaining two factors are maintained at zero.

Figure 5a shows the interaction effect between H_2SO_4 concentration and leaching temperature on V leaching efficiency. A three-dimensional surface diagram shows a curved surface with bending slopes, and the surface becomes steep with increasing H_2SO_4 concentration and leaching temperature. This is primarily because mineral dissolution requires the participation of hydrogen ions as well as anions during acid-leaching [22,23], and H^+ can efficiently remove the muscovite's structural oxygen and expose structural cations (Si/Al). HSO_4^- and SO_4^{2-} then react with Si/Al and fracture the entire muscovite structure [9]. Muscovite disintegration requires a sustained supply of heat [24]; increasing the temperature and H_2SO_4 concentration can, therefore, accelerate V-bearing mica disintegration and promote V leaching.
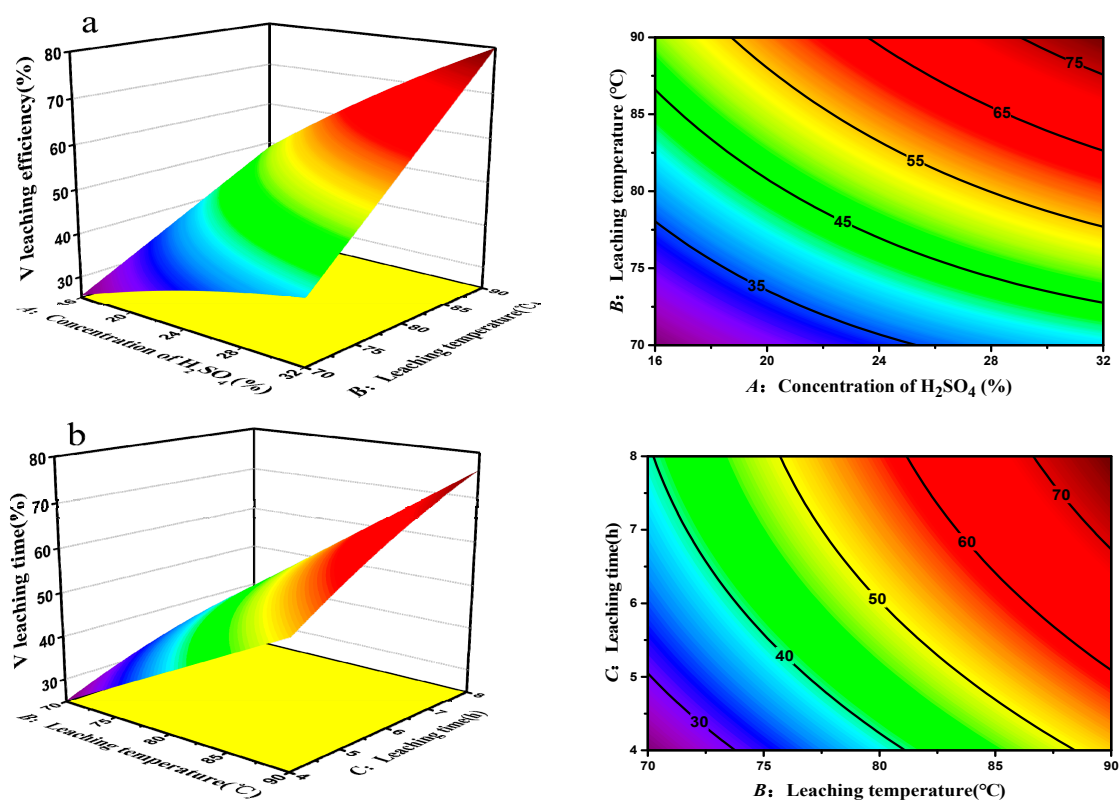

Figure 5. 3D response surface and contour plots showing the relationship between V recovery and leaching parameters (**a**,**b**). Other parameters are held at center levels.

Figure 5b shows the interaction effect between leaching temperature and leaching time on V leaching efficiency. Both time and temperature have positive effects on the OLP. The ΔG^θ (25 °C) of reactions (5)–(9) is calculated to be −228.101, −226.095, −88.458, −86.451, and −139.643 kJ/mol, respectively, using HSC chemistry 6.0 software. The above processes can be spontaneously performed from a thermodynamic viewpoint. The reaction rate of the interface is mainly controlled by two

factors analyzed from a kinetics perspective [9,25,26]: (1) the reagent diffusion rate through the product layer and (2) the reagent chemical reaction occurring on the mineral surface. According to the Stokes–Einstein equation, the diffusion coefficient is proportional to temperature [9] and higher leaching temperatures increase the diffusion rates of H^+ arriving at the muscovite surface as well as oxygen diffusion rates [27,28]. Longer leaching times lead to more MnO_2 dissociation to Mn^{2+} in the solution. The maximum V and Mn concentrations in the leach liquor were 0.012 and 0.09 mol/L, respectively. The activity of the selected dissolved state of V is, therefore, 10^{-2} and the activity of the dissolved state of Mn is 10^{-1}. The V–Mn–H_2O system at 298 K was calculated using recent information regarding the existence and free energies of various V/Mn ionic and solid species, as shown in Figure 6 [29,30]. The black lines in the diagrams represent V-H_2O, the black dotted lines describe the boundaries at which the available V is equally distributed between the two ionic species that predominate in the contiguous areas, and the red dotted lines represent Mn-H_2O systems. Oxidant MnO_2 increases the oxidation potential of the leaching environment, and under high temperatures and a strong oxidation atmosphere, low-valent V gradually transforms into V oxide ions (VO^{2+}, VO_2^+). Low-valent V oxidizes to high-valent V to constitute the soluble phase, which promotes V leaching [29,31]. The leaching temperature and time, therefore, have an interactive effect on V leaching by promoting the oxidation process of low-valent V.
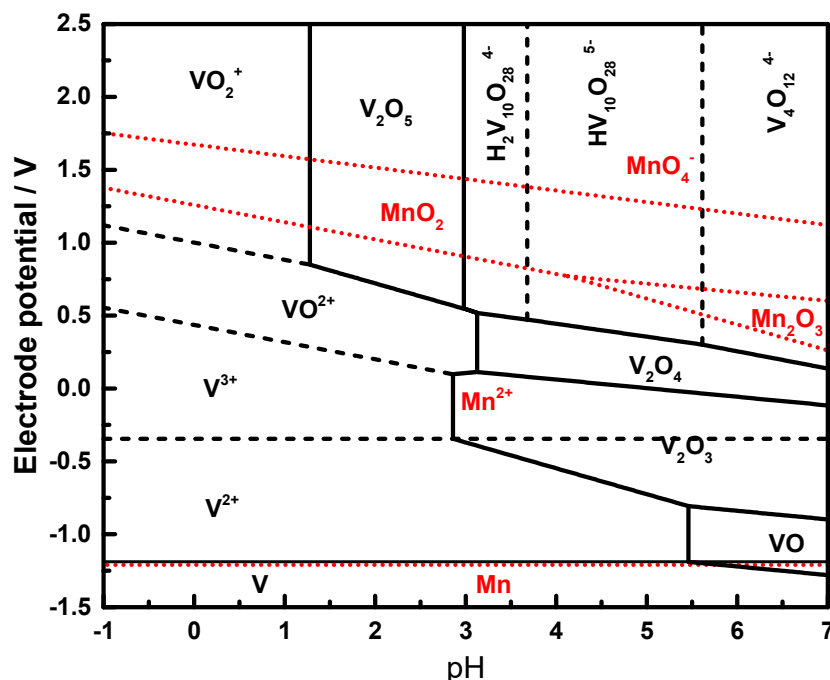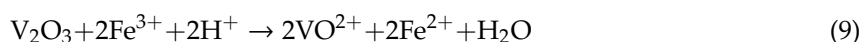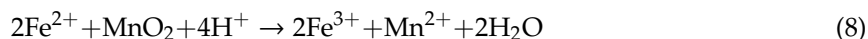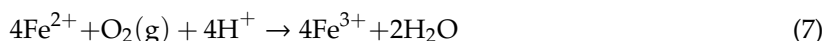
$$V_2O_3 + \frac{1}{2}O_2(g) + 4H^+ \rightarrow 2VO^{2+} + 2H_2O \tag{5}$$

$$V_2O_3 + MnO_2 + 6H^+ \rightarrow 2VO^{2+} + Mn^{2+} + 3H_2O \tag{6}$$

$$4Fe^{2+} + O_2(g) + 4H^+ \rightarrow 4Fe^{3+} + 2H_2O \tag{7}$$

$$2Fe^{2+} + MnO_2 + 4H^+ \rightarrow 2Fe^{3+} + Mn^{2+} + 2H_2O \tag{8}$$

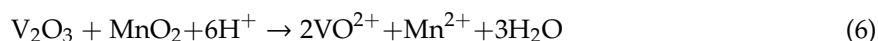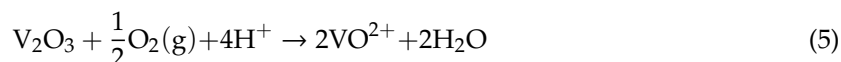$$V_2O_3 + 2Fe^{3+} + 2H^+ \rightarrow 2VO^{2+} + 2Fe^{2+} + H_2O \tag{9}$$

Figure 6. Potential-pH diagrams for the V–Mn–H_2O system with a dissolved V activity of 10^{-2} and dissolved Mn activity of 10^{-1} at 298.15 K.

3.1.4. Process Optimization

The optimum condition for V leaching efficiency was obtained by applying the RSM, as shown in Table 3 case (1)—three validation experiments confirmed that the V leaching efficiency was 88.7%, 90.1%, and 89.0% under conditions of 31% H_2SO_4 at 90 °C, leaching time of 7.9 h, and 3% MnO_2, which are consistent with the predicted value of 90.2%. Compared with the single-factor experiments without MnO_2 for leaching in cases (3) and (4), more economical and environmentally friendly optimization conditions can be obtained by modeling the OLP of stone coal and considering the interaction of various parameters.

Table 3. Case studies.

Number	H_2SO_4 Concentration (%)	Leaching Temperature (°C)	Leaching Time (h)	MnO_2 (%)	V Leaching Efficiency (%)
1	30.7166	89.9453	7.9357	2.99625	90.2
2	31	90	7.9	3	89.3
3	30	85	9	0	76.1
4	30	95	6	0	74.9

3.2. Kinetics of Leaching Process

3.2.1. Controlling Mechanism of Leaching

To confirm the leaching process, it is important to establish a quantitative measurement of the leaching kinetics and mechanism [25]. Assuming that the particles are spherical and nonporous, that ore grains gradually shrink, and that porous product layers form around unreacted grains during leaching, the experimental data can be analyzed using the shrinking core model (SCM) [25,32]. The SCM considers that the leaching process contains external diffusion control, chemical reaction control, and internal diffusion control. The results of the single-factor experiments show that the stirring speed has little effect on the V leaching efficiency so external diffusion is not a controlled-speed step. The kinetic studies, therefore, mainly focused on chemical reaction control and internal diffusion control [17,25].

Assuming the leaching process is controlled by internal diffusion, the following leaching kinetics expression can be used:

$$t = \left[1 - \frac{2}{3}\alpha - (1-\alpha)^{\frac{2}{3}}\right]/K_a \tag{10}$$

Assuming the leaching process is controlled by chemical reaction, the following expression can be applied for leaching kinetics:

$$t = \left[1 - (1-\alpha)^{\frac{1}{3}}\right]/K_b \tag{11}$$

where t is reaction time (s), α is V leaching efficiency (%), K_a is the rate constant of internal diffusion, and K_b is the rate constant of chemical reaction.

The effect of different reaction temperatures on V leaching is shown in Figure 7. The results demonstrate that α is generally low at low temperatures and significantly increases with the increase in temperature. Prolonged leaching time has no notable effect on V leaching at 60 °C. Figure 7b shows that the fitting effect of both zero point intercepts and straight $1 - (1-\alpha)^{\frac{1}{3}}$ and t is improved, and the correlation coefficient $R^2 > 0.98$, which indicates that the leaching reaction is controlled by surface chemical reactions.
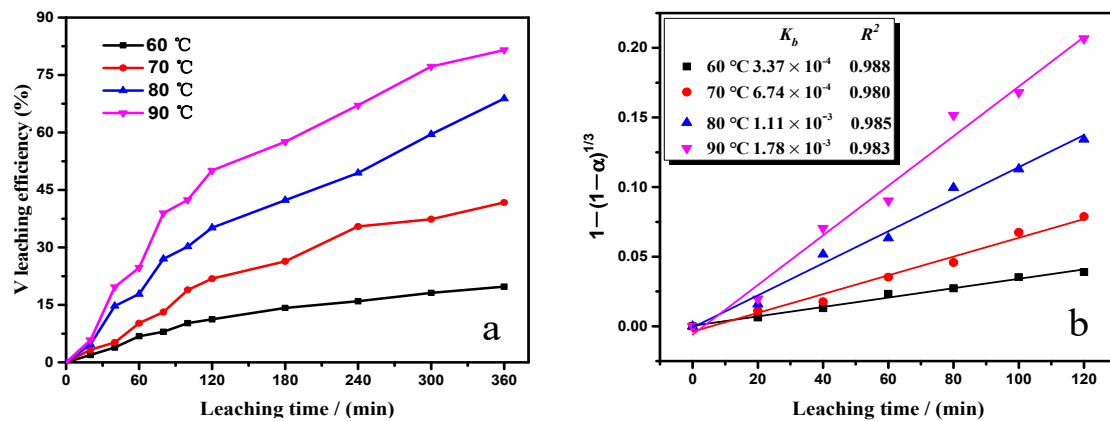
Figure 7. (**a**) Relationship between V leaching efficiency and time at different temperatures. (**b**) Plots of $1-(1-\alpha)^{1/3}$ versus time at different temperatures.

3.2.2. Determination of Activation Energy

We considered the kinetics model of the surface chemical reaction using given kinetic rate constants at studied temperatures. Figure 8 shows $\ln K_b$ vs. $1/T$ to linearize the curve fitting. The activation energy was calculated to be 55.62 kJ/mol using Equation (12), which is close to 47 kJ/mol reported for the V_2O_3 oxygen leaching process by Tavakoli et al. [28]. For chemical-controlled reactions, which are strongly dependent on reaction temperature, the activation energy is >41.8 kJ/mol [33], which supports that the OLP is controlled by chemical reaction. From the Arrhenius equation, the rate constant K is:

$$K = A \times \exp\left(-\frac{E}{RT}\right) \tag{12}$$

where E is the apparent activation energy; T is the temperature; A is the frequency factor.
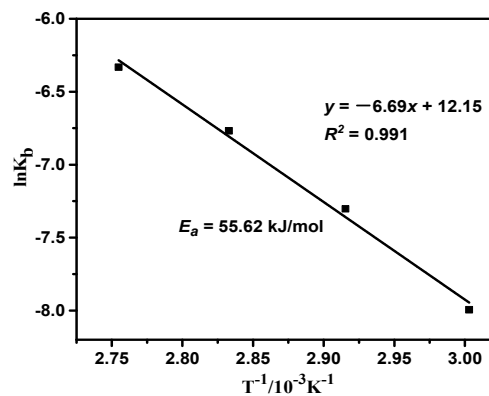

Figure 8. Relationship between $\ln K_b$ and T^{-1}.

3.2.3. Changes of the Mineral Structure before and after Leaching

SEM images of the stone coal sample and acid leaching residue are shown in Figure 9. Before leaching, the ore sample structure was very dense and most of the particles were spherical or quasi-spherical, indicating the appropriateness of the SCM model selected in the kinetic study process. The residue leached by adding MnO_2 becomes loose when the specific surface area of the ore sample increases and more readily reacts with H_2SO_4. Figure 9 shows a significant correlation between V and Al in the raw ore, and the process mineralogy of the mica-type stone coal shows an intimate association between V-bearing muscovite and other aluminosilicates [24]. However, a correlation between V and Al in the residue is not apparent and their contents clearly decrease, which indicates that the structures of muscovite and certain aluminosilicates are severely damaged and V and Al are effectively dissolved

after the OLP. Except for some aluminosilicate that was destroyed before and after leaching, most of the Si remains stable in the form of SiO_2 without reacting with sulfuric acid.
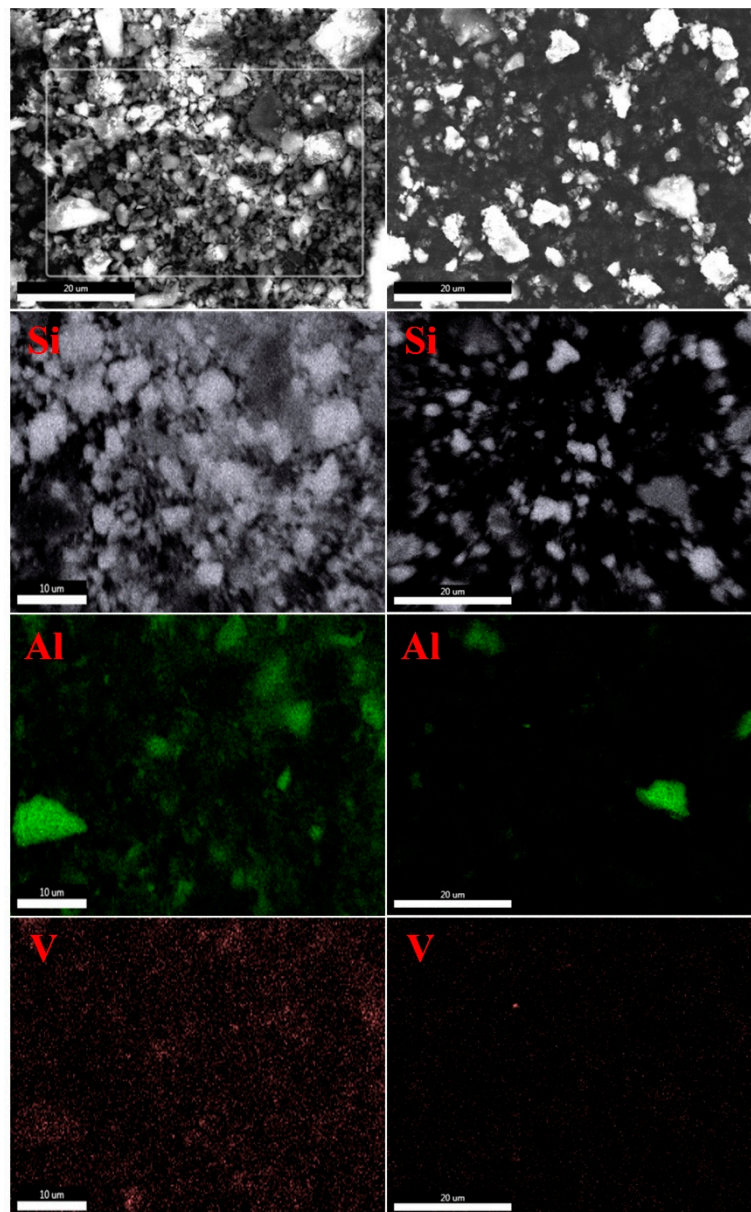

Figure 9. SEM-EDS results of the minerals before and after leaching.

4. Conclusions

V was extracted from low-grade stone coal through an OLP. RSM was used for the experimental design and optimization of V leaching, in which a statistical experimental model is suggested to model V recovery based on the studied parameters. The model results suggest that leaching temperature has the strongest influence over leaching efficiency, and the interaction between H_2SO_4 concentration and leaching temperature is the most significant. The leaching parameters were optimized in consideration of energy, chemical consumption, and leaching efficiency. Leaching conditions using 31% H_2SO_4 and 3% MnO_2 at 90 °C for 7.9 h yielded 89.3% V recovery. Chemical reaction was determined as the controlling reaction mechanism of the SCM. An Arrhenius diagram was plotted for the leaching reaction and an activation energy of 55.62 kJ/mol was obtained. SEM-EDS analysis before and after mineral leaching shows that the muscovite lattice is effectively destroyed after oxidation leaching.

Extracting vanadium through OLP does not require roasting treatment. The addition of MnO_2 can reduce the dependence of the leaching process on high temperature and strong acid concentrations. This shortens the leaching time and effectively improves the V leaching effect, which provides a low-cost and eco-friendly method for extracting vanadium from low-grade stone coal.

Supplementary Materials: The following are available online at http://www.mdpi.com/2227-9717/8/12/1534/s1, Table S1: ANOVA for RSM model for leaching of V from stone coal, Table S2: CCD matrix and response values of four variables.

Author Contributions: Conceptualization, B.Y.; Data curation, Z.H.; Formal analysis, Z.H. and W.X.; Methodology, Z.H.; Software, T.C. and Y.Z.; Supervision, T.C. and B.Y.; Validation, H.L.; Writing—original draft, Y.Z. and W.X.; Writing—review & editing, Z.H. All authors have read and agreed to the published version of the manuscript.

Conflicts of Interest: The authors declare no conflict of interest.

References

1. Wang, Z.; Chen, L.; Aldahrib, T.; Li, C.; Liu, W.; Zhang, G.; Yang, Y.; Luo, D. Direct recovery of low valence vanadium from vanadium slag—Effect of roasting on vanadium leaching. *Hydrometallurgy* **2020**, *191*, 105156. [CrossRef]

2. Yuan, Y.; Zhang, Y.; Liu, T.; Hu, P.; Zheng, Q. Optimization of microwave roasting-acid leaching process for vanadium extraction from shale via response surface methodology. *J. Clean. Prod.* **2019**, *234*, 494–502. [CrossRef]

3. Jia, L.; Zhang, Y.; Tao, L.; Jing, H.; Bao, S. A methodology for assessing cleaner production in the vanadium extraction industry. *J. Clean. Prod.* **2014**, *84*, 598–605. [CrossRef]

4. Zhang, Y.; Bao, S.; Liu, T.; Chen, T.; Huang, J. The technology of extracting vanadium from stone coal in China: History, current status and future prospects. *Hydrometallurgy* **2011**, *109*, 116–124. [CrossRef]

5. Dong, Y.; Liu, Y.; Lin, H.; Liu, C. Improving vanadium extraction from stone coal via combination of blank roasting and bioleaching by ARTP-mutated Bacillus mucilaginosus. *Trans. Nonferrous Met. Soc. China* **2019**, *29*, 849–858. [CrossRef]

6. Wang, M.; Huang, S.; Chen, B.; Wang, X. A review of processing technologies for vanadium extraction from stone coal. *Miner. Process. and Extr. Metall.* **2018**. [CrossRef]

7. Imtiaz, M.; Rizwan, M.S.; Xiong, S.; Li, H.; Ashraf, M.; Shahzad, S.M.; Shahzad, M.; Rizwan, M.; Tu, S. Vanadium, recent advancements and research prospects: A review. *Environ. Int.* **2015**, *80*, 79–88. [CrossRef]

8. Li, M.; Wei, C.; Fan, G.; Wu, H.; Li, C.; Li, X. Acid leaching of black shale for the extraction of vanadium. *Int. J. Miner. Process.* **2010**, *95*, 62–67. [CrossRef]

9. Zheng, Q.; Zhang, Y.; Liu, T.; Huang, J.; Xue, N. Vanadium extraction from black shale: Enhanced leaching due to fluoride addition. *Hydrometallurgy* **2019**, *187*, 141–148. [CrossRef]

10. Feng, Q.; He, D.; Zhang, G.; Ou, L.; Lu, Y. Effect of vanadium oxidation and conversion on vanadium leaching in extraction process of vanadium from stone coal. *Chin. J. Nonferr. Met.* **2007**, *17*, 134–138.

11. Li, M.; Wei, C.; Qiu, S.; Zhou, X.; Li, C.; Deng, Z. Kinetics of vanadium dissolution from black shale in pressure acid leaching. *Hydrometallurgy* **2010**, *104*, 193–200. [CrossRef]

12. Deng, Z.G.; WEI, C.; FAN, G.; LI, M.; LI, C.; LI, X. Extracting vanadium from stone-coal by oxygen pressure acid leaching and solvent extraction. *Trans. Nonferr. Met. Soc. China* **2010**, *20*, s118–s122. [CrossRef]

13. Kang, Y.; Zhang, X.; Tian, X.; Yang, Y.; Chen, Y. Leaching of vanadium from chromium residue. *Hydrometallurgy* **2010**, *103*, 7–11.

14. Liu, Z.; Xiang, Y.; Yin, Z.; Wu, X.; Jiang, J.; Chen, Y.; Xiong, L. Oxidative leaching behavior of metalliferous black shale in acidic solution using persulfate as oxidant. *Trans. Nonferr. Met. Soc. China* **2016**, *26*, 565–574. [CrossRef]

15. Yan, W.; Hu, L.; Gao, F.; Hua, J.; He, X. Effect of manganese dioxide on acid leaching of vanadium from stone coal. *Chin. J. Rare Met.* **2013**, *37*, 130–134.

16. Golpayegani, M.H.; Abdollahzadeh, A.A. Optimization of operating parameters and kinetics for chloride leaching of lead from melting furnace slag. *Trans. Nonferr. Met. Soc. China* **2017**, *27*, 2704–2714. [CrossRef]

17. Cai, Z.; Zhang, Y.; Liu, T.; Huang, J. Mechanisms of Vanadium Recovery from Stone Coal by Novel BaCO3/CaO Composite Additive Roasting and Acid Leaching Technology. *Minerals* **2016**, *6*, 26. [CrossRef]

18. Cao, L.; Chen, H.; Tsang, D.C.W.; Luo, G.; Hao, S.; Zhang, S.; Chen, J. Optimizing xylose production from pinewood sawdust through dilute-phosphoric-acid hydrolysis by response surface methodology. *J. Clean. Prod.* **2018**, *178*, 572–579. [CrossRef]

19. Mirazimi, S.M.J.; Rashchi, F.; Saba, M. Vanadium removal from roasted LD converter slag: Optimization of parameters by response surface methodology (RSM). *Sep. Purif. Technol.* **2013**, *116*, 175–183. [CrossRef]

20. Nazari, E.; Rashchi, F.; Saba, M.; Mirazimi, S.M. Simultaneous recovery of vanadium and nickel from power plant fly-ash: Optimization of parameters using response surface methodology. *Waste Manag.* **2014**, *34*, 2687–2696. [CrossRef]

21. Chen, F.; Zhang, Y.; Huang, J.; Liu, T.; Xue, N. Effect of manganese dioxide on direct acid leaching of extracting vanadium from stone coal. *Chem. Ind. Eng. Prog.* **2017**, *36*, 1126–1133.

22. Crundwell, F.K. The mechanism of dissolution of minerals in acidic and alkaline solutions: Part II Application of a new theory to silicates, aluminosilicates and quartz. *Hydrometallurgy* **2014**, *149*, 265–275. [CrossRef]

23. Crundwell, F.K. The mechanism of dissolution of minerals in acidic and alkaline solutions: Part VI a molecular viewpoint. *Hydrometallurgy* **2016**, *161*, 34–44. [CrossRef]

24. Zheng, Q.; Zhang, Y.; Liu, T.; Huang, J.; Xue, N. Removal Process of Structural Oxygen from Tetrahedrons in Muscovite during Acid Leaching of Vanadium-Bearing Shale. *Minerals* **2018**, *8*, 208. [CrossRef]

25. Zhu, X.; Zhang, Y.; Huang, J.; Liu, T.; Wang, Y. A kinetics study of multi-stage counter-current circulation acid leaching of vanadium from stone coal. *Int. J. Miner. Process.* **2012**, *114–117*, 1–6. [CrossRef]

26. Wang, B.; Liu, T.; Zhang, Y.; Huang, J. Effect of CaF2/CaO Composite Additive on Roasting of Vanadium-Bearing Stone Coal and Acid Leaching Kinetics. *Minerals* **2017**, *7*, 43. [CrossRef]

27. Tromans, D. Oxygen solubility modeling in inorganic solutions: Concentration, temperature and pressure effects. *Hydrometallurgy* **1998**, *50*, 279–296. [CrossRef]

28. Tavakoli, M.R.; Dreisinger, D.B. The kinetics of oxidative leaching of vanadium trioxide. *Hydrometallurgy* **2014**, *147–148*, 83–89. [CrossRef]

29. Chen, B.; Huang, S.; Liu, B.; Ge, Q.; Xie, S.; Wang, M.; Wang, X. Thermodynamic analysis for separation of vanadium and chromium in V(IV)–Cr(III)–H2O system. *Trans. Nonferr. Met. Soc. China* **2018**, *28*, 567–573. [CrossRef]

30. Zhou, X.; Wei, C.; Li, M.; Qiu, S.; Li, X. Thermodynamics of vanadium–sulfur–water systems at 298K. *Hydrometallurgy* **2011**, *106*, 104–112. [CrossRef]

31. Peng, H.; Liu, Z.; Tao, C. Leaching Kinetics of Vanadium with Electro-oxidation and H_2O_2 in Alkaline Medium. *Energy Fuels* **2016**, *30*, 7802–7807. [CrossRef]

32. Pritzker, M.D. Shrinking-core model for systems with facile heterogeneous and ho-mogeneous reactions. *Chem. Eng. Sci* **1996**, *51*, 3631–3645. [CrossRef]

33. Ju, Z.; Wang, C.; Yin, F. Dissolution kinetics of vanadium from black shale by activated sulfuric acid leaching in atmosphere pressure. *Int. J. Miner. Process.* **2015**, *138*, 1–5. [CrossRef]

Publisher's Note: MDPI stays neutral with regard to jurisdictional claims in published maps and institutional affiliations.